Received: 16 December 2020 | Revised: 19 March 2021 | Accepted: 26 April 2021

DOI: 10.1049/bsb2.12008

Biosurface and Biotribology

The Institution of Engineering and Technology WILEY

ORIGINAL RESEARCH PAPER

Raman analysis of chemisorbed tribofilm for metal-on-polyethylene hip joint prostheses

Risha Rufaqua[1] | Martin Vrbka[1] | Dušan Hemzal[2] | Dipankar Choudhury[3] | David Rebenda[1] | Ivan Křupka[1] | Martin Hartl[1]

[1]Faculty of Mechanical Engineering, Brno University of Technology, Brno, Czech Republic

[2]Department of Condensed Matter Physics, Faculty of Science, Masaryk University, Brno, Czech Republic

[3]Nano Mechanics and Tribology Laboratory, Department of Mechanical Engineering, University of Arkansas, Fayetteville, Arkansas, USA

Correspondence

Risha Rufaqua, Faculty of Mechanical Engineering, Brno University of Technology, Technická 2896/2, 616 69 Brno, Czech Republic.
Email: Risha.Rufaqua@vut.cz

Funding information

Ministry of Education, Youth and Sports of the Czech Republic, Grant/Award Number: FSI-S-20-6443; GrantovÃ¡ Agentura ÄŒeskÃ© Republiky, Grant/Award Number: 20-00483S

Abstract

The biochemical reaction during the formation of lubricant film the in case of a cobalt-chromium ball on an ultrahigh-molecular weight polyethylene cup was studied. Three types of model synovial fluids and hyaluronic acid (HA) at physiologic concentrations were used in the experiment. The coefficient of friction was measured using a pendulum hip simulator, and Raman spectroscopy was used to perceive chemical reactions between the synovial fluid and implant material. Raman spectra evidenced that the three model fluids and HA chemisorbed onto the cobalt-chromium surface. An α-helix structure of the model fluid components was detected on the surface of the prosthesis.

1 | INTRODUCTION

In clinical applications, Co–Cr alloys are used in the form of wrought and cast alloys. In combination with polyethylene, Co–Cr alloys have been effectively used to fabricate artificial disc prostheses. Co–Cr–Mo alloy (ASTM F75) was introduced in hip prostheses during the late 1960s. This alloy is widely used in orthopaedic implants such as hip and knee joint replacements [1]. Owing to mechanically enhanced electrochemical processes, Co–Cr–Mo alloys release ions into the human body. This tribocorrosion is strongly affected by biological reactions. Moreover, protein-lubricated metal-on-metal (MoM) sliding contact is predicted to undergo tribochemical reactions, which significantly improve performance. A protective layer is formed by the reaction, called a carbonaceous tribofilm. Scanning electron microscopy and Raman spectroscopy results revealed that the formation of the tribofilm is influenced by the contact load. Thus, the film is postulated to be protective, facilitating the reduction of material loss during sliding. Proteins have a vital role in this tribochemical reaction; they are contained within the synovial fluid (SF) of human joints, together with other organic components such as hyaluronic acid (HA) and lubricin [2, 3].

The impact of the protein content of model SFs on film formation under static and rolling conditions was studied by Parkes et al. [4]. Two different pH ranges and six different compositions of SFs were used to track the film thickness and kinetics of formation. It was confirmed that the film formation depends on the protein content and pH of the solution under both conditions. Protein layers were thicker under rolling than static conditions. Bovine γ-globulin deposits were thicker compared with bovine serum albumin (BSA). For low pH, relaxed protein adsorption was noticed in the initial stage, whereas the adsorption rate increased with time. A thicker non-uniform and irregular deposition protein film formed under rolling conditions was observed at pH 7.4 or lower. At the primary stage, viscoelasticity is higher with a higher pH and under static conditions, and a uniform and consistent film was formed [5]. Because of the presence of protein, the total specific wear rate increased under abrasion corrosion test conditions. Correspondingly, the formation of metal–protein complexes was predicted in bovine serum solutions at an enhanced corrosion rate [6]. The formation of a passivation film on the Co–Cr–Mo orthopaedic alloy was studied in a simulated physiologic solution by X-ray photoelectron spectroscopy. The formation of a

complex layer was observed using electrochemical oxidation, in which the applied potential manipulated both the composition and thickness of the formed film [7]. Using the electrochemical method, the area of adsorption and the frictional property of BSA under rubbing conditions with ultrahigh-molecular weight polyethylene (UHMWPE) and Co–Cr–Mo alloy were explored in situ. Using real-time information about the adsorption and desorption of proteins, it was disclosed that during rubbing, the BSA film is reconstructed on the Co–Cr–Mo surface by shear force. By acquiring shear force, the adsorbed film becomes a strong, stable and optimally adapted structure [8]. Electrochemical corrosion resistance is a vital factor in the biocompatibility of metals. Within the body's environment, surgical alloys achieve exceptionally high electrochemical corrosion resistance. To improve the biocompatibility of metal components further, a reduction of metal ion release is anticipated [9]. Interfacial and bulk rheology for model SF were studied for various shear rates, strains and frequencies as an effect caused by proteins and HA. In the steady and oscillatory condition of the model SF composed from HA, BSA and γ-globulin, at the interface interfacial rheology are rejected due to protein adsorption. On the other hand, bulk rheology was controlled wholly by HA in model SF for various shear rates, strains and frequencies [10]. In another study, two distinct mechanisms of film formation were studied: boundary lubrication and a high-viscosity gel mechanism. As agglomerated protein forms organic deposits on the surface of implants, wear is inflicted through tribocorrosion; with higher pH, wear increases. The chemistry within SF has a substantial impact on the wear and failure of joint replacement [11]. Concerning the lubrication of Co–Cr–Mo hip prostheses, the influence of BSA and γ-globulin concentration was researched along with the frictional coefficient. It was revealed that sufficient boundary lubrication is maintained by maximum BSA levels and an optimal concentration of γ-globulin. Thus, the concentrations of BSA and γ-globulin control the friction of the Co–Cr–Mo head. Optimal concentrations can be manipulated to increase the lubricating ability of Co–Cr–Mo hip prostheses by altering the surface roughness and coating of the bearing surface [12]. Boundary lubrication ability was also determined for the retrieved Co–Cr–Mo head regarding HA and phospholipids, along with microscale frictional coefficients. The retrieved Co–Cr–Mo head's microscale frictional response depends on the concentration of HA and phospholipids. The optimal concentration to maximise lubrication is similar to the concentration of HA and dipalmitoylphosphatidylcholine of human SF [13]. The contribution to boundary lubrication of various constituents of SF separately and collectively was also studied. Graded concentrations of SF constituents (HA, proteoglycan 4 and surface-active phospholipids) and their combinations were used for cartilage boundary lubrication tests. At both physiologic and pathophysiologic concentrations, the constituents of SF contribute to boundary lubrication of the articular cartilage surface. The contribution was specified individually and for the combined SF constituents [14]. In addition, HA and glycoprotein lubricin (LUB) form a complex HA-LUB, trapped at the interface to form a cross-linked network, which has a role as a boundary lubricant and prevents wear [15].

Necas et al. [16] conducted spectroscopic studies of film formation on implants; a Co–Cr–Mo and polyethylene contact pair had a coefficient of friction dependent on both the protein concentration and kinematic conditions for an albumin and γ-globulin mixture. Film thickness and the structure of the adsorbed proteins were evaluated using spectroscopic ellipsometry and Fourier transform infrared spectroscopy, respectively. The total protein concentration and adsorbed film thickness noticeably affect friction. Also, the structure of the protein adsorbed on the UHMWPE surface has an impact on kinematic conditions on the frictional behaviour of the contact couple. The native structure of adsorbed molecules was retained at a high sliding speed, whereas denaturation of adsorbed proteins was found when the sliding speed was lower. Cr–Co–Mo hip joint prostheses with micro-dimples in bovine serum lubricant developed remarkably increased film thicknesses and a shortened transition period [17]. Infrared reflection-absorption spectroscopy analysis during a wear test of Co–Cr–Mo material pairs showed deposits formed predominately by proteins, suggesting denaturation of the proteins. During rubbing, denatured proteins turned out to be adherent. Thus, the rubbing process forms insoluble agglomerates that are deposited and contribute to reduced wear [18]. Consequently, surface protection during rubbing is contributed by insoluble, denatured protein films as a primary lubrication mechanism [19]. For model fluids, a higher concentration of HA and phospholipids causes a reduction in film thickness in the case of the metal head [20]. In addition, compared with ceramic heads, metal heads form thicker films during articulation [21]. Concerning the effect of friction, the implant material is a fundamental parameter. Usually, friction is increased twice by implementing the metal pair compared with ceramic. In the case of hard-on-hard pairs, adding protein to the lubricant exposed a positive result for friction, whereas adding protein to the hard-on-soft pairs elicited almost no response [22].

Not many studies concentrate on the biochemical composition of synovial joints, in which spectroscopic technique was used for analysis. Using Raman spectroscopy, variations in molecular structures between tibial plateaus of healthy joints and joints with total replacements resulting from osteoarthritis were evaluated. Also, medial and adjacent compartments of subchondral bones were compared at different load-bearing sites [23]. An investigation of differences between the biochemical compositions of healthy joint SF and the SF of osteoarthritis patients was carried out in Esmonde-White et al. [24]. Galandakova et al. [25] revealed that adsorption of albumin and γ-globulin on artificial materials takes place instantaneously, also affecting the frictional properties of the lubricating surface. It is necessary to observe the biochemical reactivity of SF on implant materials to increase the depth of knowledge on joint replacement procedures and enhance the longevity of orthopaedic implants. Studying different synovial components in appropriate ratios, instead of using bovine serum, may uncover more practical results to understand lubrication chemistry and the mechanism of SF within the prosthesis [26]. Therefore, the objective of this

study is to observe chemical structural changes in SF components and implant materials within joint replacements.

2 | MATERIALS AND METHODS

2.1 | Pendulum hip simulator

The pendulum hip simulator is an exclusive and unique biotribological instrument that imitates the flexion and extension of artificial hip joints together with their real geometry, body temperature and loads. It is efficient in measuring the real-time velocity profile, average friction coefficients and viscous effect (an indicator of lubrication film formation). Vrbka et al. [27] conducted an experiment with this simulator to visualise lubricating films between an artificial head and cup in real geometry. Necas et al. [21] used the same instrument to understand the effect of diameter, clearance and material during an in situ observation of lubricant film formation. Choudhury et al. used this simulator to understand a significant reduction in friction coefficient for a dimpled a-C:H/ceramic prosthesis compared with a metal (CoCr)/ceramic prosthesis. The results indicated that the simulator can be used as an advanced biotribometer [21, 27, 28].

The simulator is composed of a base frame with the acetabular cup and a swinging pendulum with a femoral head. The pendulum is driven by electromagnetic motors that allow continuous motion in the flexion-extension plane [21]. The schematic diagram of pendulum hip joint simulator is shown in Figure 1. This kind of instrumental setup may help determine chemical reactions within SF after artificial joint replacement, as well as the frictional coefficient of individual contact pairs.

2.2 | Ball-on-cup configuration

To clarify lubrication processes within artificial joints, the experiments were conducted in a ball-on-cup configuration, in which the contact couple was Co–Cr–Mo (the ball) and polyethylene (the acetabular cup). In particular, the metal hip prosthesis head of a Co–Cr–Mo ball (28 mm) from Zimmer was used in accordance with ISO 5832-12, which contains cobalt-chromium casting alloy. The cup was made from polyethylene by Smith and Nephew (28 mm).

2.3 | Model fluid lubricants

To observe the chemical reaction occurring within hip replacement, three types of model SFs were used as lubricants in the ball-on-cup configuration. These model fluids were prepared with concentrations of components at real physiologic values, as evaluated by Galandakova et al. [25]. In particular, the three types of model fluids are the mimic of SF of healthy or physiologic joint (SF1), SF of total joint replacement (SF2) and SF within a joint with osteoarthritis (SF3) [25, 29]. In the model fluids, the concentrations of albumin, γ-globulin, HA and phospholipids were maintained within the range observed in human joints, as described in Table 1.

Albumin, γ-globulin, HA and phospholipids were dissolved in phosphate-buffered saline with a laboratory rocker-shaker overnight (MR-12, Biosan, Riga, Latvia) at 4°C. The next step of preparation was mixing individual components into model fluids in the order: albumin, γ-globulin, HA, phospholipids. The lubricant solutions were preserved at −22°C after preparation.

Product specifications of the applied components applied are: BSA (powder, ≥96%, A2153, Sigma-Aldrich, St. Louis, MO, USA), γ-globulin from bovine blood (powder, >99%, G5009, Sigma-Aldrich), HA (sodium hyaluronate HySilk, powder, quality class cosmetic, molecular weight 820–1020 kDa, Contipro, Dolní Dobrouc, Czech Republic), and phospholipids (L-α-phosphatidylcholine, powder, type XVI-E, lyophilised powder, >99%, vesicles form, P3556, Sigma-Aldrich.

Albumin (28.0 mg/ml) and γ-globulin (11.0 mg/ml) were also used as lubricants separately with the Co–Cr–Mo ball in our previous experiment [26]. These two lubricants are used individually in this experiment to determine the coefficient of friction within the contact pair. HA (2.0 mg/ml) was tested to observe the chemical reaction occurring with the metal contents of the Co–Cr–Mo ball.

To observe the tribological effect within the pendulum hip joint simulator, each experiment was conducted for 5–6 min to achieve chemical changes on the ball surface. After the tribological experiment, fluid was collected for analysis. All experiments were performed at 37°C. We used 532 N load for our experiment. The range in deviation of the pendulum for flexion-extension swinging was −16° to +16°; maximum Hertzian contact pressure was 29 MPa. Velocity and rotation are linearly damped sinusoidal functions of frequency at 0.5 Hz.

2.4 | Raman spectroscopy

Raman spectroscopy is a fast and non-destructive method for the characterisation and structure analysis of chemical compounds and bonds [30]. Raman spectroscopy provides information about the chemical structure of compounds through the identification and analysis of functional groups [31]. Therefore, Raman spectroscopy is a qualitative technique to determine the structure and dynamics of biological molecules [32]. Differences in Raman spectra acquired for each lubricant before use and after the experiment within the simulator show that chemical reactions are taking place within the artificial joint replacement. Through Raman spectra, the obtained vibrational fingerprints demonstrate the specific chemical structure of individual lubricant components within the formed films [26].

To obtain the fingerprints of different lubricants before and after the tribological experiment in the simulator, a Renishaw inVia Raman spectrometer was used at 532 nm excitation. After the tribological test, the Co–Cr–Mo ball and lubricants were preserved at 4°C for 24 h; afterwards, Raman

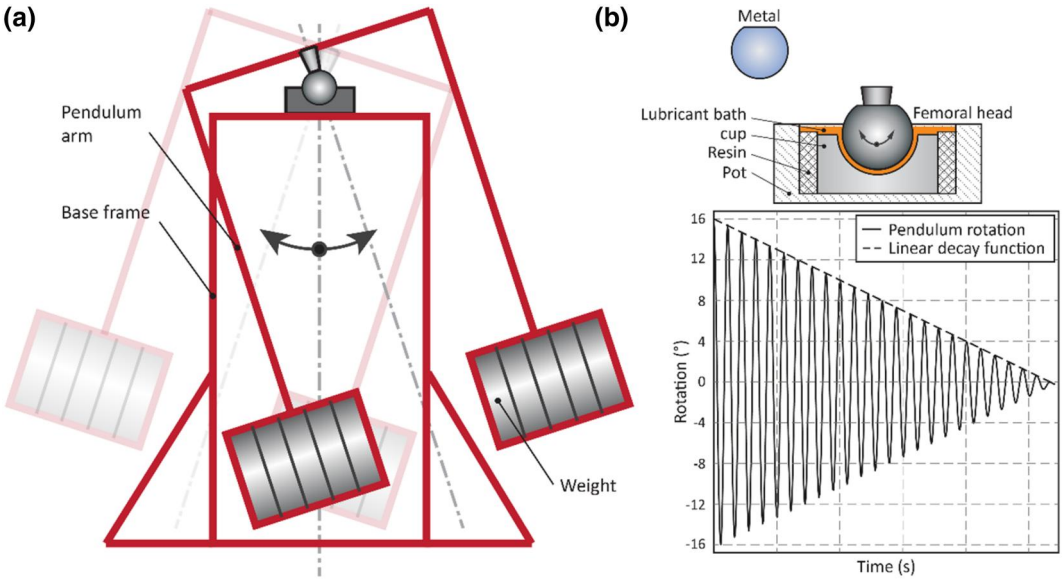

FIGURE 1 (a) Schematic illustrating the pendulum hip joint simulator; (b) Overview of tested femoral components, detail of the contact couple, and representative linear decay signal

TABLE 1 Composition and concentration of applied test lubricants

Test Fluid	Albumin (mg/ml)	γ-globulin (mg/ml)	Hyaluronic Acid (mg/ml)	Phospholipid (mg/ml)
Healthy joint (SF1)	20	3.6	2.5	0.15
After total joint replacement (SF2)	26.3	8.2	0.87	0.35
Joint with osteoarthritis (SF3)	24.9	6.1	1.49	0.34
Hyaluronic acid			2	

analysis was conducted. The surfaces of the balls were observed to determine chemical changes resulting from the tribological process. On the surface of Co–Cr–Mo ball, 1 mW of laser power was used with a total exposure of 100 s. Fingerprints of the lubricants before and after tribological tests were achieved with 100 mW laser power and 20 s exposure.

2.5 | Coefficient of friction measurement

The coefficient of friction for the Co–Cr–Mo and polyethylene contact pair was also determined for each lubricant. Within the pendulum hip joint simulator, the acetabular cup is installed using resin in a stainless-steel pot. This setup is mounted to the base frame. The swinging arm is connected to the head using a cone. Measurement of friction coefficient was realized by evaluating the viscous damping effect from the angular velocity profiles by a novel pendulum hip joint simulator. The concept of the evaluation of friction coefficient from a pendulum velocity profile was first reported by Crisco et al. [33] When the experiment starts, the pendulum arm is deflected to the primary position and then released. The flexion-extension swinging motion with a constant deflection lasted for 5 min. After this, the pendulum drive was shut down and the swinging motion was damped only by friction within contact. Instant deflection of the pendulum is recorded by an angular velocity sensor. Consequently, the recorded signal is evaluated using a linear model of damping to obtain the friction coefficient [34]. Thus, the friction coefficient was derived from a curve of slowing pendulum oscillations. This method was previously used to determine the friction coefficient [28, 34–36]. Therefore, we measured angular velocity by the difference in maximum and minimum deflection to determine the linear decay function.

3 | RESULTS

3.1 | Raman analysis

The Co–Cr–Mo surface before and after the tribological test with different model fluids resulted in Raman spectra shown in Figure 2. The spectra for model fluid SF1 and SF3 showed peaks at 1659 cm^{-1}, whereas for SF2 it shifted to 1654 cm^{-1}. Another peak was seen at 1443 cm^{-1}, 1446 cm^{-1} and 1448 cm^{-1} for SF1, SF2 and SF3, respectively, for the film on the surface. SF2 and SF3 on the surface showed peaks at 1340 cm^{-1} and 1333 cm^{-1}, respectively, whereas SF1 had no peaks in this range. A peak at 1001 cm^{-1} was found for all three lubricants.

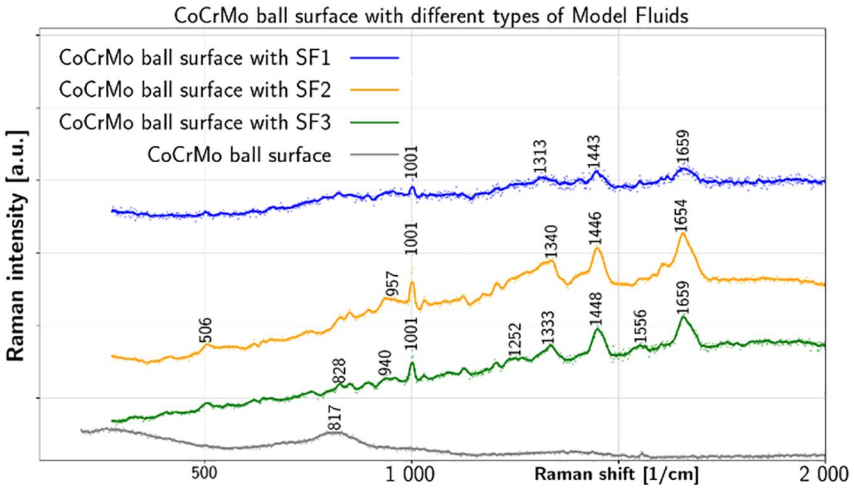

FIGURE 2 Raman spectroscopic data of Co–Cr–Mo ball surface with SF1, SF2, and SF3, respectively

SF1 liquid spectra without a test and after the test with Co–Cr–Mo are compared in Figure 3. Before the test, SF1 showed a prominent peak at 1651 cm^{-1}, which shifted after the tribological test to 1654 cm^{-1}. Peaks at 1449 and 1336 cm^{-1} shifted to 1451 and 1340 cm^{-1} after the test, whereas the peak near 1210 cm^{-1} and the sharp peak near 1003 cm^{-1} remained essentially unchanged. The peak at 945 cm^{-1} before testing was positioned at 953 cm^{-1} after the test. Finally, a broader band near 450 cm^{-1} was observed in both spectra. SF2 liquid spectra without a test and after the test with Co–Cr–Mo are compared in Figure 4; most of the data for this figure are comparable to those of Figure 3 for SF1. Without a test, the SF2 prominent peak at 1656 cm^{-1} was at 1651 cm^{-1} for SF1, whereas after the test with the metal ball, both fluids exhibited this peak at 1654 cm^{-1}. The pretest SF2 peaks at 1451 and 1336 cm^{-1} shifted after the test to 1449 and 1338 cm^{-1}, respectively. The peak near 1210 cm^{-1}, which was present in SF1 spectra, was absent for SF2 liquid. Again, a sharp peak was observed both before and after the test SF2 at 1003 cm^{-1}. The peak at 945 cm^{-1} before the test shifted to 943 cm^{-1} after test for SF2 liquid, similar to SF1. A broader band was visible around 490 cm^{-1} both before and after the test for SF2 liquid.

Raman spectra of SF3 liquid before and after the tribological test with Co–Cr–Mo are presented in Figure 5. Several peaks in Figure 5 are comparable to those of Figures 3 and 4 for SF1 and SF2 liquids, respectively. Before testing, the SF3 prominent peak at 1656 cm^{-1} was in the same position for SF2, but for SF1 the peak shifted to 1651 cm^{-1}. Nevertheless, all three model fluids show this peak after the test with Co–Cr–Mo at 1654 cm^{-1}. SF3 pretest peaks at 1456 and 1340 cm^{-1} shifted to 1451 and 1341 cm^{-1}, respectively, after the test. The peaks in these two ranges were also visible for SF1 and SF2 liquids. The sharp peak at 1004 cm^{-1} and the one at 943 cm^{-1} remained essentially unaffected by the test and thus were visible for all three fluids. Finally, a broader band near 450 cm^{-1} was seen for SF3 fluid both before and after the test.

The Raman spectra of HA liquid without a test and after the test with Co–Cr–Mo are compared in Figure 6. Both without and with the test, HA displayed double peaks near 1400 and 1100 cm^{-1}. In particular, the peak component at 1090 cm^{-1} in pretest liquid shifted to 1079 cm^{-1} after the test. The strong peak at 992 cm^{-1} was present both before and after the test HA liquid. The Co–Cr–Mo surface spectra are illustrated in Figure 7 both before and after the tribological test with HA acid. The spectrum found for the after-test surface is entirely different from that before the test. The clean Co–Cr–Mo surface provides peaks at 1555, 1384, 817 and 688 cm^{-1}, whereas after the test with HA, metal surface peaks are visible near 1465, 1408, 1051 and 950 cm^{-1}.

3.2 | Microscopic view of formed films

Figures 8, 9 and 10 provide microscopic photos of the film formed on the Co–Cr–Mo ball with SF1, SF2 and SF3. In Figure 8, the Co–Cr–Mo surface after the tribological experiment with SF1 (the model SF of a healthy joint) shows no noticeable film structure. In contrast, SF2 in Figure 9 (the model SF after total joint replacement) shows a thick and branched film. A similar branched pattern of film was also found in our previous experiment with albumin and γ-globulin film on the Co–Cr–Mo surface [26]. Consequently, these films result from protein accumulation on the metal surface. Raman spectra were taken for both the branched and flat areas of the Co–Cr–Mo surface with SF2. The branched area provided more substantial Raman peaks than did the flat area. Similarly, in Figure 10, SF3 forms a branched film on the metal surface, but the pattern was not as apparent as for SF2. The type of model fluid changes the characteristics of the film on the metal ball surface: when concentrations of the SF elements change, so does the pattern of the developed film. Figure 11 shows the film on Co–Cr–Mo formed by HA. It also exhibits some kind of pattern, but the pattern was not visible on the metal surface before Raman measurement.

3.3 | Coefficient of friction analysis

The friction coefficient of all three types of model fluid with a Co–Cr–Mo ball was above 0.23. The highest value of 0.2365

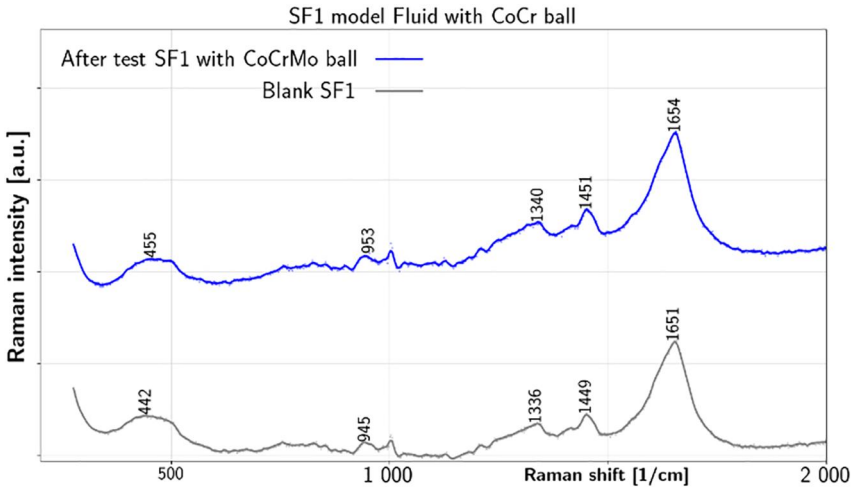

FIGURE 3 Raman spectroscopic data for SF1 model synovial fluid liquid before and after the test with Co–Cr–Mo

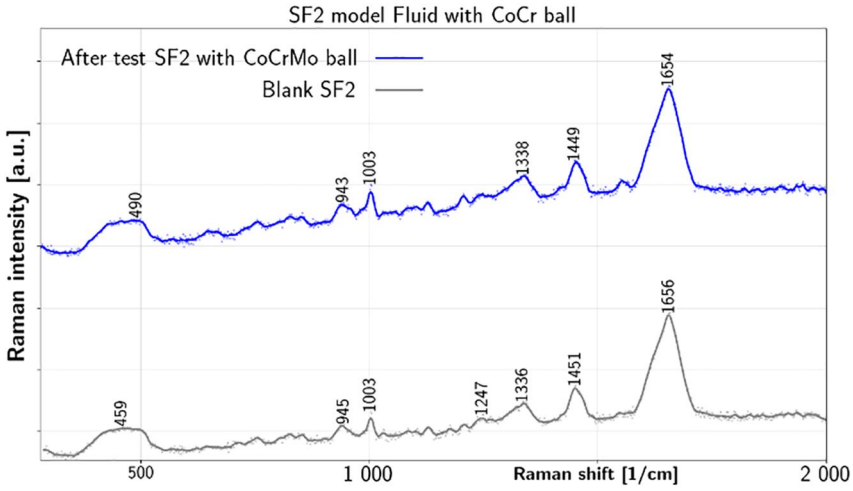

FIGURE 4 Raman spectroscopic data for SF2 model synovial fluid liquid before and after test with Co–Cr–Mo

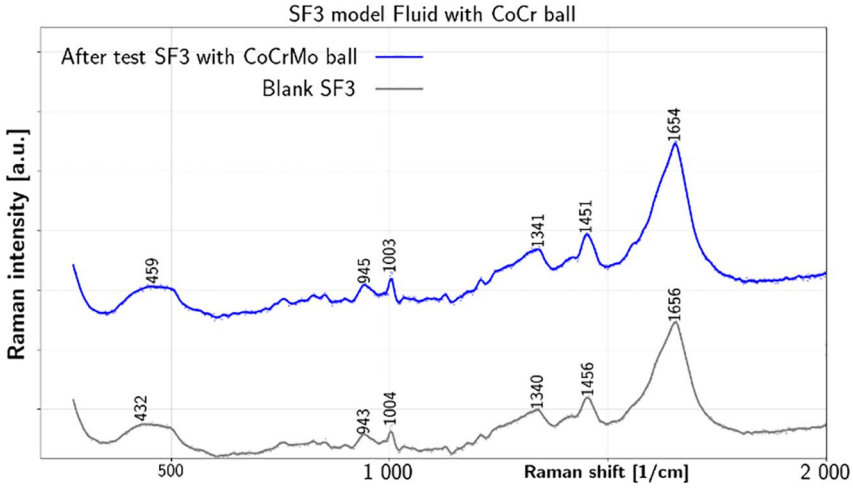

FIGURE 5 Raman spectroscopic data for SF3 model synovial fluid liquid before and after test with Co–Cr–Mo

was shown by SF2, and the lowest value was 0.2308 for SF1. When measuring the coefficient of friction separately for the components (albumin, γ-globulin and HA), all values were lower than that of the model SFs. HA had a coefficient of friction as low as 0.072, whereas γ-globulin had the highest value of 0.208 among the SF components. In the Co–Cr–Mo ball and polyethylene cup setup, albumin had a coefficient of friction of 0.1969. The values are listed in Figure 12.

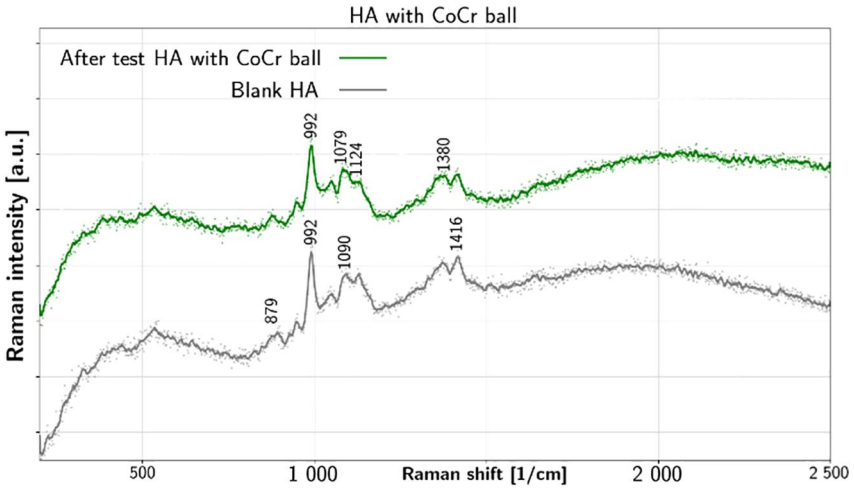

FIGURE 6 Raman spectroscopic data for hyaluronic acid liquid before and after test with Co–Cr–Mo

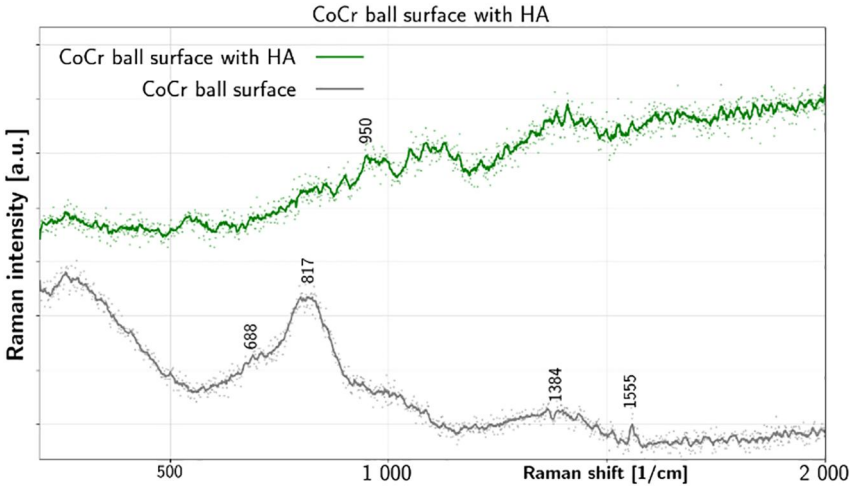

FIGURE 7 Raman spectroscopic data of Co–Cr–Mo ball surface with hyaluronic acid liquid

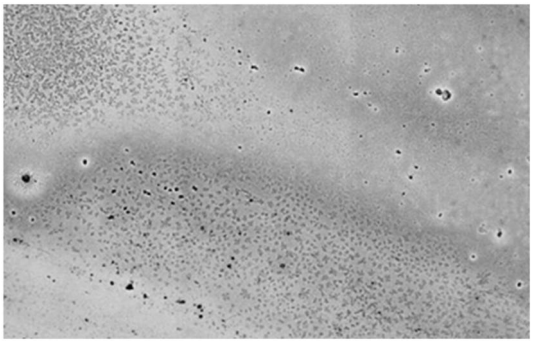

FIGURE 8 Co–Cr–Mo ball viewed by Raman microscope SF1 on the surface. The horizontal size of the panel is 20 μm

4 | DISCUSSION

This work aims to clarify chemical reactions taking place among several model SFs and Co–Cr–Mo joint replacement during the formation of tribofilm, and to study the frictional properties. To track the state of the SF components, vibrational fingerprints provided by Raman spectroscopy were used.

The Raman analysis of the Co–Cr–Mo surface after the tribological test with all model fluids is described subsequently. The prominent peak near 1660 cm^{-1} is due to water; it is found at 1659 cm^{-1} for model fluids SF1 and SF3, whereas for SF2 it shifted to 1654 cm^{-1}. However, because these positions constitute a significant shift from the usual water peak position at 1642 cm^{-1}, it is possible that convolution with amide I band for α-helix, within 164-51660 cm^{-1} [32], takes place, which could facilitate albumin adsorption on the Co–Cr–Mo surface for the model fluids we used. The peaks at 1443, 1446 and 1448 cm^{-1} for SF1, SF2 and SF3, respectively, resulted from CH_2/CH_3 deformation [24, 37]. In addition, SF2 and SF3 exhibited peaks at 1340 and 1333 cm^{-1}, respectively. This range provides information regarding CH_2-CH_3 wagging [24, 37]. It is noticeable that SF1 did not provide a peak near this area. SF3 also provides a peak near 1280 cm^{-1}, which is within the α-helix range of the amide III band [32], which supports the conclusion that from SF3, albumin adsorbs onto Co–Cr–Mo. In comparison, SF2 exhibits a peak near 1123 cm^{-1}, in the range of protein backbone vibrations: C–C, C–OH, C–N stretch, C–O–C and glycosidic linkage [24]. All three fluids on Co–Cr–Mo have a sharp peak near 1000 cm^{-1},

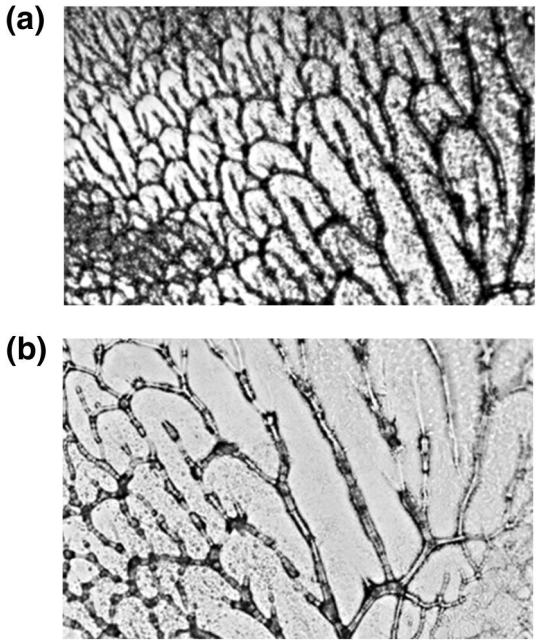

FIGURE 9 Co–Cr–Mo ball viewed by Raman microscope SF2 on the surface. The horizontal sizes of the panels are 20 μm (a) and 5 μm (b)

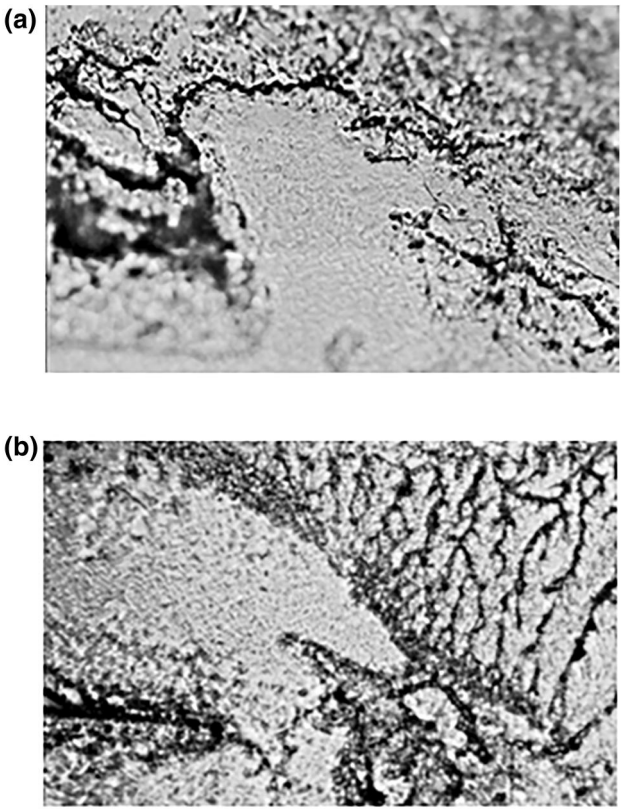

FIGURE 10 Co–Cr–Mo ball viewed by Raman microscope SF3 on surface. The horizontal sizes of the panels are 20 μm (a) and 5 μm (b)

which is due to benzene ring breathing [24, 37]. The peak near 850 cm^{-1} provided on the surface by SF2 and SF3, respectively, is in the range of C–C skeletal stretch [37, 38]; it is not provided by SF1. Because these peaks do not match peaks of the Co–Cr–Mo substrate and several α-helix related features were observed, we suggest that adsorption of (mainly helical) albumin to the Co–Cr–Mo surface takes place from all model fluids. In addition, SF3 (which mimics an osteoarthritic joint) is attached with more bonds to Co–Cr–Mo surface than SF1, whereas for SF2 (mimicking the SF of total joint replacement) protein backbone vibrations were also detected. The maximum amount of albumin is present in SF2 (i.e., in the model fluid of total joint replacements), but the ratio of the model fluid components present in SF3 (osteoarthritic SF) is more favourable for film formation on the Co–Cr–Mo surface. In diseased joints, the amount of protein is naturally altered [25] and more protein is involved in forming the film on the metal surface. The film changes on the surface of Co–Cr–Mo, particularly for SF2 and SF3, are also remarkable in the microscopic pictures. SF2 forms a branched film, and it seems from the microscopic pictures that SF3 also forms a thicker film compared with SF1.

Raman spectra of SF1 liquid with Co–Cr–Mo present before testing and after the test show water peaks at 1651 and 1654 cm^{-1}, respectively, which seem to include a contribution from α-helix amide I band [32], as described earlier. The peak at 1449 cm^{-1} before testing shifted to 1451 cm^{-1} after the test; it is in the range of CH_2/CH_3 deformation [24, 37]. In contrast, the peak provided by SF1 at 1336 cm^{-1} before testing and at 1340 cm^{-1} after the test is caused by CH_2-CH_3 wagging [24, 37]. The C–C stretching region [39] is covered by the peak near 1200 cm^{-1} before testing and after the test, respectively. The benzene ring breathing peak at 1003 cm^{-1} appears for both SF1 liquids without shifting [39]. The SF1 liquid peak at 945 cm^{-1} before testing that shifted to 953 cm^{-1} after the test is in the range of α-helix C–C skeletal stretching [39]. The peak at 442 cm^{-1} before testing and at 455 cm^{-1} after the test shows C–C skeletal deformation [37]. SF2 liquid before testing and after the test shows similarities to SF1 liquid data. The water peak range 1645–1660 cm^{-1} seems to include the α-helix amide I band contribution [32]. The CH_2/CH_3 deformation peak [24, 37] is visible for SF2 before testing at 1451 cm^{-1}, and after the test at 1449 cm^{-1}. The SF2 peak at 1338 cm^{-1} after the test, which appeared at 1336 cm^{-1} before testing, expresses CH_2-CH_3 wagging [24, 37]. The benzene ring breathing mode peak [39] is visible for both SF2 liquids at 1003 cm^{-1}. The C–C skeletal stretching of α-helix [39] is proven in SF2 by the presence of the peak at 945 cm^{-1} before testing and at 943 cm^{-1} after the test. Thus, Figures 3 and 4 for SF1 (healthy SF) and SF2 (SF after joint replacement) are comparable. Raman spectra of SF3 before testing and after the tribological process in Figure 5 are also equivalent to Figures 3 and 4 (SF1) and (SF2). The SF3 water peak including α-helix amide I band contribution was found at 1656 cm^{-1} before testing and at 1654 cm^{-1} after the test. Similar to SF1 and SF2, the peak providing information on CH_2/CH_3 deformation is present for SF3 at 1456 cm^{-1} before testing and at 1451 cm^{-1} after the test. Moreover, SF3 CH_2-CH_3 wagging appears at 1340 cm^{-1}

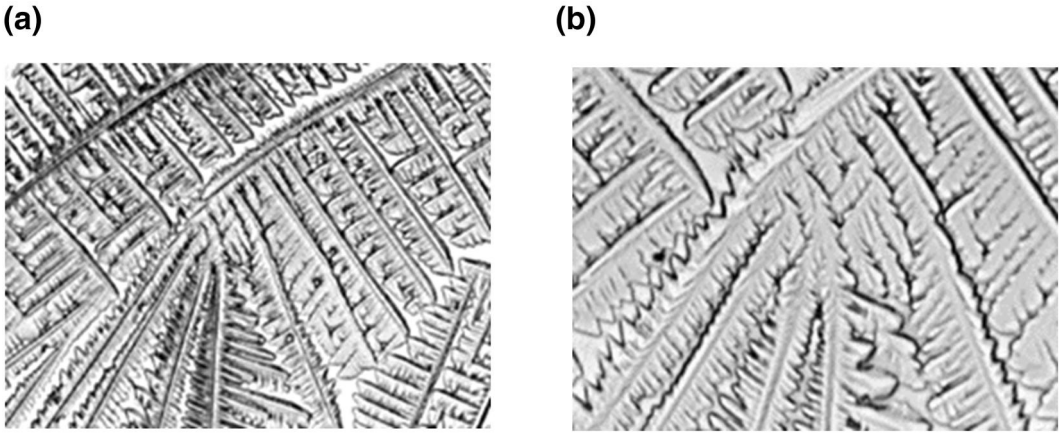

FIGURE 11 Co–Cr–Mo ball viewed by Raman microscope after test with hyaluronic acid. The horizontal sizes of the panels are 20 μm (a) and 5 μm (b)

FIGURE 12 Coefficient of friction for Co–Cr–Mo and polyethylene contact pairs for albumin, γ-globulin, hyaluronic acid and SF1, SF2 and SF3 model synovial fluid

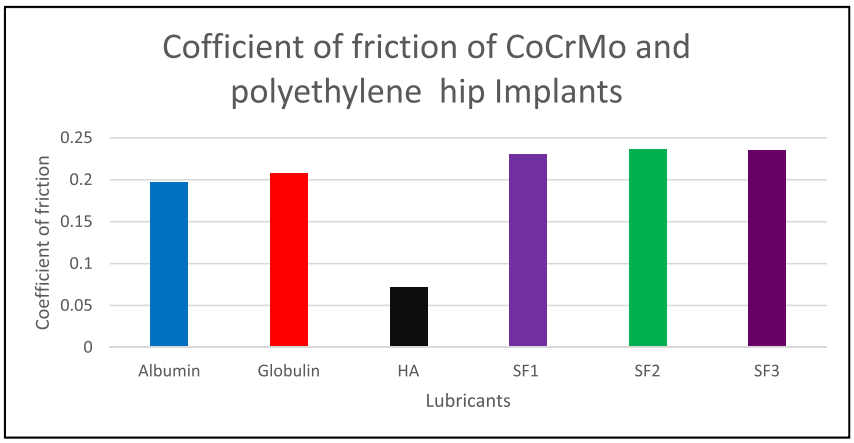

before testing and at 1341 cm^{-1} after the test. The weak SF3 liquid peak in the 1270 cm^{-1} range is found both before and after the test. Consequently, we assign this peak to the α-helix range (1265–1300) of the amide III band [32]. The C–C stretching [39] in SF3 is attributed to the peak near 1210 cm^{-1} after the test, similar to SF1. The SF3 benzene ring breathing mode has a peak near 1003 cm^{-1} both before and after the test. The α-helix C–C skeletal stretching is observed at 943 cm^{-1} before testing and at 945 cm^{-1} after the test for SF3 liquid. The peak near 850 cm^{-1} provides information on C–C skeletal stretch [37, 38]. In addition, the peak at 432 cm^{-1} before testing and at 459 cm^{-1} after the test indicates C–C skeletal deformation [37].

Turning to HA, liquid before and after the test with Co–Cr–Mo (in Figure 6) exhibits similar characteristics. The double peak near 1400 cm^{-1} is caused by C–N stretching and C–H deformation. The peak at 1090 cm^{-1} before testing and at 1079 cm^{-1} after the test is due to the C–OH bend in the acetyl group [38, 40]. The sharp HA peak at 992 cm^{-1} is due to ring breathing [37], and the additional peak at 879 cm^{-1} is observable in other literature [38]. After the test, HA has a peak at 1380 cm^{-1}, which provides information about C–H bend [38]. Another peak is noticeable after the test at 1124 cm^{-1}, which could be the result of C–C stretch [37]. The Co–Cr–Mo surface exhibited Raman peaks at 155, 1384, 817 and 688 cm^{-1}. Not much literature was found for the characteristics of these peaks. Liao et al. [41] describe peaks at 1383 and 1567 cm^{-1} as correlated to disordered sp2-carbon and sp3-bonded carbon in Co–Cr–Mo. However, the spectra of the Co–Cr–Mo surface observed after the tribological test with HA varied from those of the clean surface. The surface after the test exhibited a peak near 1400 cm^{-1}, which in literature is the result of C–N stretching and C–H deformation [38, 40]. Another peak of the surface after the test near 1050 cm^{-1} is likely due to C–C and C–O stretching [38, 40]. Finally, the peak near 1465 cm^{-1} demonstrates CH_3 deformation within the Co–Cr–Mo surface [37]. Observing the film thickness of HA on Co–Cr–Mo implants, Necas et al. [20] concluded that HA is not an effective lubricant on Co–Cr–Mo. In Figure 7, HA after the test shows metal surface peaks due to C–N stretching and C–H deformation, C–C and C–O stretching, and CH_3 deformation. Thus, it can be predicted that, when using HA at physiologic concentration alone, its chemisorption takes place on the Co–Cr–Mo surface. Non-destructive electrochemical measurements of Co–Cr–Mo in synovial model fluid containing physiologically relevant concentrations of albumin and HA were also evaluated. A complexation of degenerated HA molecular chains with chromium ions released from the

metallic surface was postulated, which may decrease corrosion resistance of the alloy. This attribution is described as essential to building the protective oxide film. Therefore, corrosion of Co–Cr–Mo implants is enhanced by HA in the presence of strong inflammation [42].

In our experiments, HA peaks are not observed in the spectra of the model fluids, and no surface of Co–Cr–Mo with SF1, SF2 and SF3 model fluids showed peaks relevant to HA. Thus, all spectra for the model fluids were missing an HA contribution, which agrees with results by Esmonde et al., who used Raman spectroscopy to assess SF in both healthy and osteoarthritic patients [24]. Nevertheless, HA formed a patterned film on Co–Cr–Mo when the tribological test was executed separately for HA. In a study of MoM hip retrievals, electrochemically induced film formation showed the presence of carbonaceous tribofilms derived from synovial proteins, particularly on articulating surfaces. It is evident that the films decrease corrosion and wear, and thus are potentially able to increase the corrosion resistance of biomedical implants. However, it is suggested that mechanical characterisation is necessary to estimate the total performance of the generated film [43].

The coefficient of friction calculated for all model fluids with a Co–Cr–Mo ball and polyethylene cup is higher than the frictional coefficient of the proteins and HA separately. In addition, HA had a lower coefficient of friction compared with the other components. Although the molecular weight of HA has a vital impact on its rheological properties, the HA molecular weight and its coefficient of friction had no mutual dependency [44]. Also, only a limited effect on friction was found when protein-based lubricants were applied varying the fluid constituent concentration in the range corresponding to physiologic and osteoarthritic SF [29]. A dependence between the coefficient of friction for model fluids, proteins and HA with chemical changes of Co–Cr–Mo could not be identified.

5 | CONCLUSIONS

This research provides a joint study of frictional and chemical conditions occurring within artificial joint replacement. Raman spectroscopy was used to determine the chemisorption of model fluids on the Co–Cr–Mo ball surface. Simultaneously, the frictional coefficient was measured to reveal the relationship with chemical reactions. Key results from the investigation were that:

- Chemisorption occurs on the Co–Cr–Mo surface with all three types of model SF representing physiologic, total joint replacement and osteoarthritic SF and also with HA as a separate lubricant.
- When using albumin, γ-globulin, HA and phospholipid concentrations appropriate for healthy humans, total joint replacement and a joint with osteoarthritis SF, model fluids attach chemically to the Co–Cr–Mo surface through proteins rather than HA.
- Vibrational traces of α-helix structure are found on the surface of Co–Cr–Mo, which favours albumin as a binding protein.
- Model SFs emulating osteoarthritic joints and joints after replacement are chemically more adsorbable to the Co–Cr–Mo surface than SF imitating a healthy joint; the film formed using these two SF types is distinctly visible under the microscope.
- The coefficient of friction with the Co–Cr–Mo ball and polyethylene cup had a higher value for all model fluids than for protein and HA separately. The lowest coefficient of friction was obtained for HA.
- The coefficient of friction for model fluids, proteins or HA could not be significantly correlated with chemical changes of Co–Cr–Mo.

The use of various model fluids within a ball-on-cup configuration provided clear information about the chemistry of lubricant film formation. Furthermore, the methodology enables an observation of chemical reactions of specific components of SF with the implant material. Thus, this procedure can be exploited to determine the chemical changes within artificial hip implants to introduce improved implant materials.

ACKNOWLEDGEMENTS

This research was carried out under Project 20-00483S with financial support from the Czech Science Foundation, and under Project FSI-S-20-6443 with financial support from the Ministry of Education, Youth, and Sports of the Czech Republic.

ORCID

Risha Rufaqua https://orcid.org/0000-0002-2261-966X

REFERENCES

1. Navarro, M., et al.: Biomaterials in orthopaedics. J R Soc Interface. 5(27), 1137–1158 (2008)
2. Wimmer, M.A., et al.: The effect of contact load on CoCrMo wear and the formation and retention of tribofilms. Wear. 332-333, 643–649 (2015)
3. Yan, Y., Neville, A., Dowson, D.: Biotribocorrosion of CoCrMo orthopaedic implant materials—assessing the formation and effect of the biofilm. Tribol Int. 40(10-12), 1492–1499 (2007)
4. Parkes, M., et al.: Synovial fluid lubrication: the effect of protein interactions on adsorbed and lubricating films. Biotribology. 1-2, 51–60 (2015)
5. Parkes, M., et al.: The effect of buffer solution choice on protein adsorption and lubrication. Tribol Int. 72, 108–117 (2014)
6. Sun, D., et al.: Microabrasion-corrosion of cast CoCrMo alloy in simulated body fluids. Tribol Int. 42(1), 99–110 (2009)
7. Milošev, I., Strehblow, H.H.: The composition of the surface passive film formed on CoCrMo alloy in simulated physiological solution. Electrochim Acta. 48(19), 2767–2774 (2003)
8. Nakashima, K., et al.: Behaviour of adsorbed albumin film on CoCrMo alloy under in-situ observation. Tribol Online. 10(2), 183–189 (2015)
9. Dorner-Reisel, A., et al.: Electrochemical corrosion behaviour of uncoated and DLC coated medical grade Co28Cr6Mo. Surf Coating Technol. 177-178, 830–837 (2004)

10. Zhang, Z., Barman, S., Christopher, G.F.: The role of protein content on the steady and oscillatory shear rheology of model synovial fluids. Soft Matter. 10(32), 5965–5973 (2014)
11. Fan, J., et al.: Synovial fluid lubrication of artificial joints: protein film formation and composition. Faraday Discuss. 156(1), 69–85 (2012)
12. Duong, C.T., et al.: Effect of protein concentrations of bovine serum albumin and γ-globulin on the frictional response of a cobalt-chromium femoral head. J Mater Sci Mater Med. 23(5), 1323–1330 (2012)
13. Park, J.B., et al.: Role of hyaluronic acid and phospholipid in the lubrication of a cobalt–chromium head for total hip arthroplasty, pp. 204–219. Biointerphases. 9(3), 031007 (2014)
14. Schmidt, T.A., et al.: Boundary lubrication of articular cartilage: role of synovial fluid constituents. Arthritis Rheum. 56(3), 882–891 (2007)
15. Greene, G.W., et al.: Adaptive mechanically controlled lubrication mechanism found in articular joints. Proc Natl Acad Sci Unit States Am. 108(13), 5255–5259 (2011)
16. Nečas, D., et al.: The influence of proteins and speed on friction and adsorption of metal/UHMWPE contact pair. Biotribology. 11, 51–59 (2017)
17. Choudhury, D., et al.: Enhanced lubricant film formation through micro-dimpled hard-on-hard artificial hip joint: an in-situ observation of dimple shape effects. J. Mech. Behav. Biomed. Mater. 81, 120–129 (2018)
18. Stevenson, H., et al.: The development of a small-scale wear test for CoCrMo specimens with human synovial fluid. Biotribology. 14, 1–10 (2018)
19. Stevenson, H., et al.: The role of denatured synovial fluid proteins in the lubrication of artificial joints. Biotribology. 17, 49–63 (2019)
20. Nečas, D., et al.: In situ observation of lubricant film formation in THR considering real conformity: the effect of model synovial fluid composition. Tribol Int. 117, 206–216 (2018)
21. Nečas, D., et al.: In situ observation of lubricant film formation in THR considering real conformity: the effect of diameter, clearance and material. J. Mech. Behav. Biomed. Mater. 69, 66–74 (2017)
22. Nečas, D., et al.: The effect of kinematic conditions and synovial fluid composition on the frictional behaviour of materials for artificial joints. Materials. 11(5), 767 (2018)
23. Kerns, J.G., et al.: Evidence from Raman spectroscopy of a putative link between inherent bone matrix chemistry and degenerative joint disease. Arthritis & Rheumatology. 66(5), 1237–1246 (2014)
24. Esmonde-White, K.A., et al.: Raman spectroscopy of synovial fluid as a tool for diagnosing osteoarthritis. J Biomed Opt. 14(3), 034013 (2009)
25. Galandáková, A., et al.: Characteristics of synovial fluid required for optimization of lubrication fluid for biotribological experiments. J Biomed Mater Res. 105(6), 1422–1431 (2017)
26. Rufaqua, R., et al.: A systematic review on correlation between biochemical and mechanical processes of lubricant film formation in joint replacement of the last 10 years. Lubric Sci. 31(3), 85–101 (2019)
27. Vrbka, M., et al.: Visualization of lubricating films between artificial head and cup with respect to real geometry. Biotribology. 1-2, 61–65 (2015)
28. Choudhury, D., et al.: A novel tribological study on DLC-coated micro-dimpled orthopaedics implant interface. J. Mech. Behav. Biomed. Mater. 45, 121–131 (2015)
29. Furmann, D., et al.: The effect of synovial fluid composition, speed and load on frictional behaviour of articular cartilage. Materials. 13(6), 1334 (2020)
30. Papež, N., et al.: Degradation analysis of GaAs solar cells at thermal stress. Appl Surf Sci. 461, 212–220 (2018)
31. Depciuch, J., et al.: Phospholipid-protein balance in affective disorders: analysis of human blood serum using Raman and FTIR spectroscopy. A pilot study. J Pharmaceut Biomed Anal. 131, 287–296 (2016)
32. Diem, M.: Modern vibrational spectroscopy and micro-spectroscopy: theory, instrumentation and biomedical applications. John Wiley & Sons, pp. 204–219. Hoboken (2015)
33. Crisco, J.J., et al.: Assuming exponential decay by incorporating viscous damping improves the prediction of the coeffcient of friction in pendulum tests of whole articular joints. Proc Inst Mech Eng H. 221(3), 325–333 (2007)
34. Nečas, D., et al.: Running-in friction of hip joint replacements can be significantly reduced: the effect of surface-textured acetabular cup. Friction. 8(6), 1137–1152 (2020).
35. Vrbka, M., et al.: Determination of a friction coefficient for THA bearing couples. Acta Chir Orthop Traumatol Cech. 82(5), 341–347 (2015)
36. Choudhury, D., et al.: The impact of surface and geometry on coefficient of friction of artificial hip joints. J. Mech. Behav. Biomed. Mater. 72, 192–199 (2017)
37. Lin-Vien, D., et al.: The handbook of infrared and Raman characteristic frequencies of organic molecules. Elsevier Amsterdam, Netherlands (1991)
38. Essendoubi, M., et al.: Human skin penetration of hyaluronic acid of different molecular weights as probed by Raman spectroscopy. Skin Res Technol. 22(1), 55–62 (2016)
39. Chourpa, I., et al.: Conformational modifications of α gliadin and globulin proteins upon complex coacervates formation with gum Arabic as studied by Raman microspectroscopy. Biomacromolecules. 7(9), 2616–2623 (2006)
40. Kotzianová, A., et al.: Raman spectroscopy analysis of biodegradable electrospun nanofibers prepared from polymer blends. Monatsh Chem. 147(5), 919–923 (2016)
41. Liao, Y., et al.: CoCrMo metal-on-metal hip replacements. Phys Chem Chem Phys. 15(3), 746–756 (2013)
42. Radice, S., et al.: The effect of hyaluronic acid on the corrosion of an orthopaedic CoCrMo-alloy in simulated inflammatory conditions. Materialia. 6, 100348 (2019)
43. Kerwell, S., et al.: Electrochemically induced film formation on CoCrMo alloy for hip implant application. J. Bio-and Tribo-Corrosion. 3(1), 4 (2017)
44. Rebenda, D., et al.: On the dependence of rheology of hyaluronic acid solutions and frictional behaviour of articular cartilage. Materials. 13(11), 2659 (2020)

How to cite this article: Rufaqua, R., et al.: Raman analysis of chemisorbed tribofilm for metal-on-polyethylene hip joint prostheses. Biosurface and Biotribology. 1–11 (2021). https://doi.org/10.1049/bsb2.12008